



Universiteit  
Leiden  
The Netherlands

## **Systems pharmacology of the amyloid cascade : unfolding oligomer modulation in Alzheimer's disease**

Maanen, E.M.T. van

### **Citation**

Maanen, E. M. T. van. (2017, November 23). *Systems pharmacology of the amyloid cascade : unfolding oligomer modulation in Alzheimer's disease*. Retrieved from <https://hdl.handle.net/1887/55514>

Version: Not Applicable (or Unknown)

License: [Licence agreement concerning inclusion of doctoral thesis in the Institutional Repository of the University of Leiden](#)

Downloaded from: <https://hdl.handle.net/1887/55514>

**Note:** To cite this publication please use the final published version (if applicable).

Cover Page



Universiteit Leiden

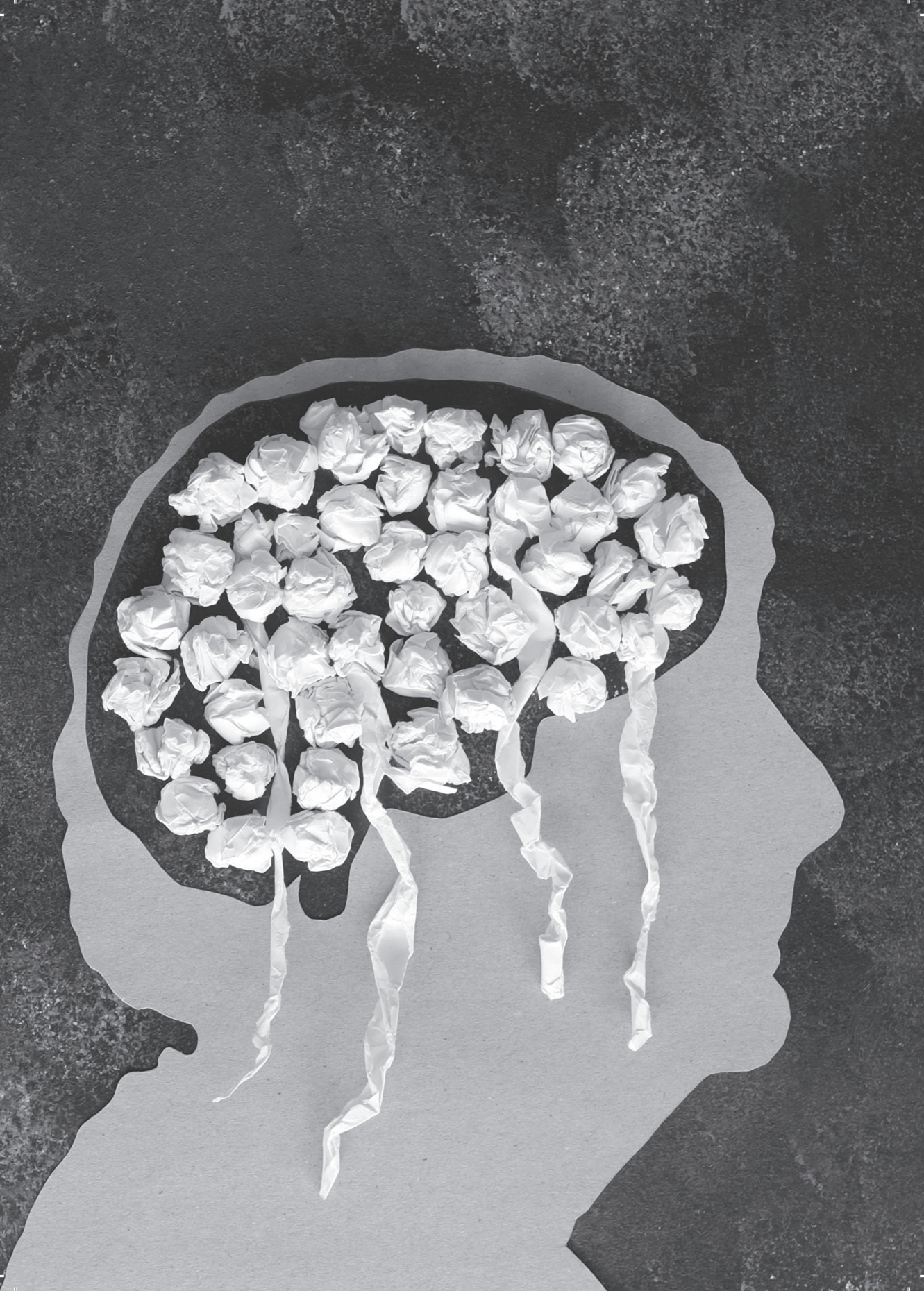


The handle <http://hdl.handle.net/1887/55514> holds various files of this Leiden University dissertation.

**Author:** Maanen, E.M.T. van

**Title:** Systems pharmacology of the amyloid cascade : unfolding oligomer modulation in Alzheimer's disease

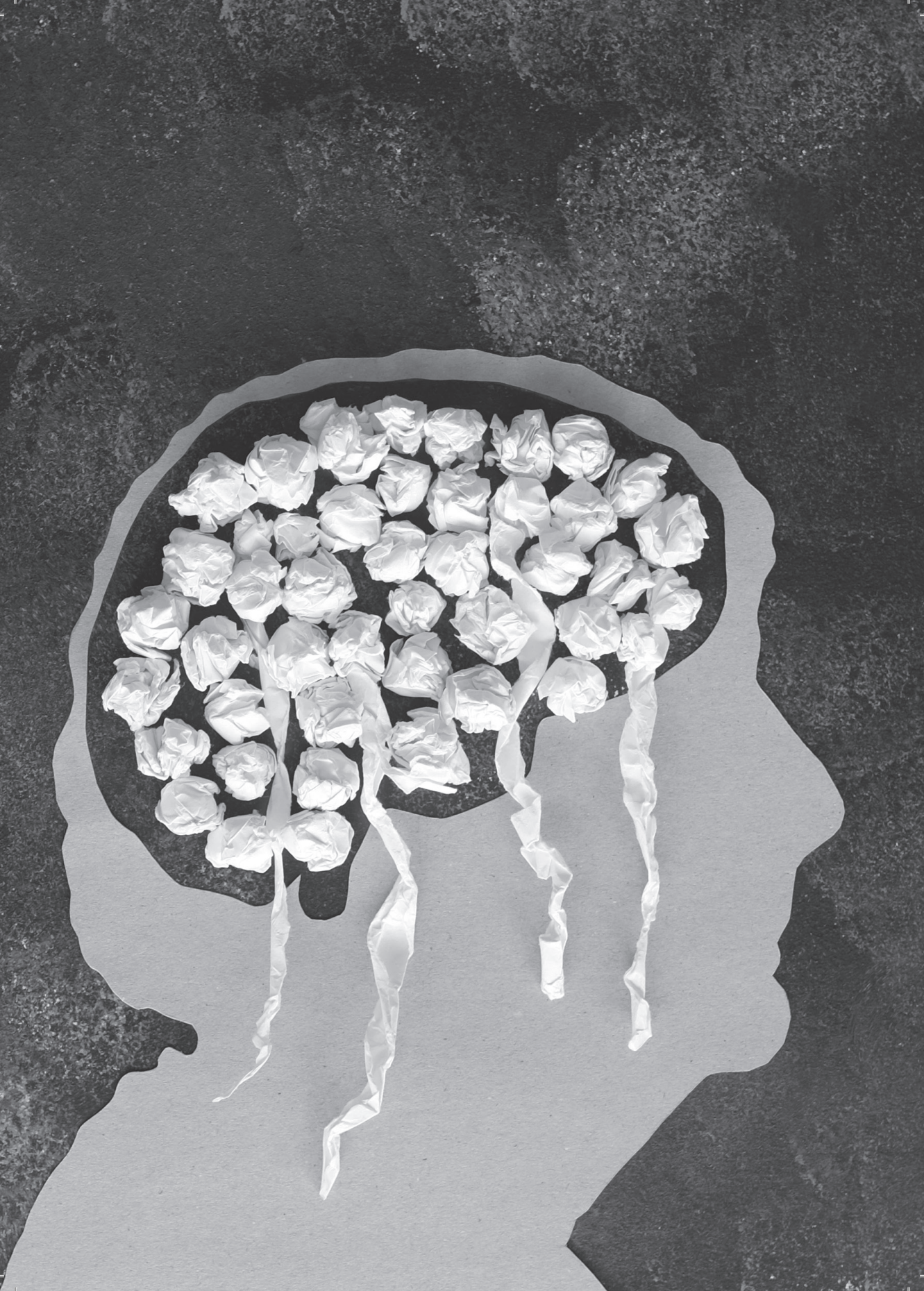
**Issue Date:** 2017-11-23





# *Section II*

Development of a systems pharmacology model  
to predict oligomer response following  
secretase inhibition



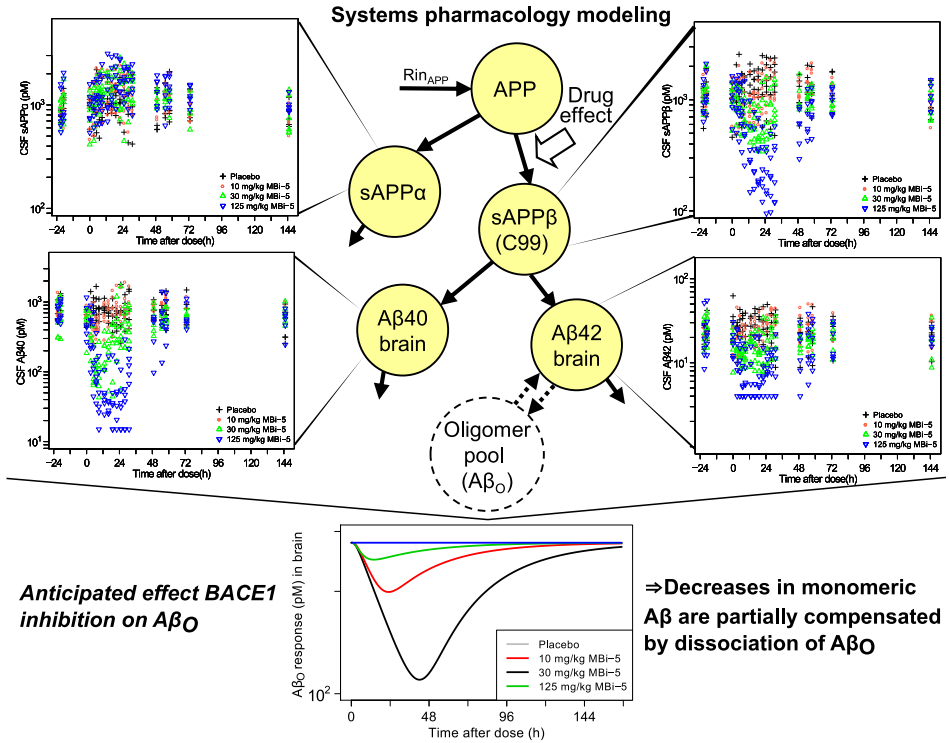


# *Chapter 3*

Systems pharmacology analysis of the amyloid cascade following  $\beta$ -secretase inhibition enables the identification of an A $\beta$ 42 oligomer pool

E.M.T. van Maanen, T.J. van Steeg, M.S. Michener, M.J. Savage,  
M.E. Kennedy, H.J. Kleijn, J.A. Stone, M. Danhof

Visual Abstract



## **Abstract**

The deposition of amyloid- $\beta$  oligomers in brain parenchyma has been implicated in the pathophysiology of Alzheimer's disease. Here we present a systems pharmacology model describing the changes in the amyloid precursor protein (APP) pathway following administration of three different doses (10, 30 and 125 mg/kg) of the  $\beta$ -secretase (BACE1) inhibitor MBI-5 in cisterna magna ported rhesus monkeys. The time course of the MBI-5 concentration in plasma and cerebrospinal fluid (CSF) was analysed in conjunction with the effect on the concentrations of the APP metabolites  $A\beta_{42}$ ,  $A\beta_{40}$ , sAPP $\alpha$  and sAPP $\beta$  in CSF. The systems pharmacology model contained expressions to describe the production, elimination and brain-to-CSF transport for the APP metabolites. Upon the administration of MBI-5 a dose dependent increase of the metabolite sAPP $\alpha$  and dose dependent decreases of sAPP $\beta$  and  $A\beta$  were observed. Maximal inhibition of BACE1 was close to 100% and the value of the IC<sub>50</sub> was 0.0256  $\mu$ M (95% CI, 0.0137-0.0375). A differential effect of BACE1 inhibition on  $A\beta_{40}$  and  $A\beta_{42}$  was observed, with the  $A\beta_{40}$  response being larger than the  $A\beta_{42}$  response. This enabled the identification of an  $A\beta_{42}$  oligomer pool in the systems pharmacology model. These findings indicate that decreases in monomeric  $A\beta$  responses resulting from BACE1 inhibition are partially compensated by dissociation of  $A\beta$  oligomers and suggest that BACE1 inhibition may also reduce the putatively neurotoxic oligomer pool.



## Introduction

The amyloid cascade hypothesis posits that amyloid- $\beta$  protein ( $A\beta$ ) peptide levels are increased early in Alzheimer's Disease (AD) leading to the formation of toxic soluble  $A\beta$  oligomers ( $A\beta_O$ ) and plaques<sup>1</sup>. According to this hypothesis, a series of causal events initiated by abnormal  $A\beta$  levels leads to neuronal cell death and cognitive and functional decline over time<sup>2</sup>. Toxic  $A\beta_O$  are considered to be the drivers of the neurodegeneration<sup>3,4</sup>. Such soluble forms of multimeric  $A\beta$  peptides are intermediate of soluble  $A\beta$  monomers and insoluble  $A\beta$  fibrils and likely consist of a mixture of oligomeric species.  $A\beta$  dimers, trimers, larger  $A\beta_O$  and structures such as soluble protofibrils have been isolated from AD brain<sup>5,6,7,8</sup>.  $A\beta_O$  are in a constant equilibrium with  $A\beta$  monomers and other  $A\beta$  aggregates<sup>3</sup>.

Formation of  $A\beta$  requires proteolytic cleavage of the transmembrane protein '  $\beta$ -amyloid precursor protein' (APP). Sequential cleavage of APP by the enzymes  $\beta$ -secretase (BACE1) and  $\gamma$ -secretase leads to the formation of  $A\beta^9$ , as schematically depicted in 3.1. Here cleavage by BACE1 leads to the formation of both the N-terminal secreted fragment soluble APP $\beta$  (sAPP $\beta$ ) and the C-terminal membrane-bound 99-amino acid fragment (C99). C99 is subsequent subject to cleavage by  $\gamma$ -secretase yielding  $A\beta$  species of different chain length. The most common  $A\beta$  isoforms have 38 ( $A\beta_{38}$ ), 40 ( $A\beta_{40}$ ) or 42 ( $A\beta_{42}$ ) amino acids<sup>10</sup>. In parallel full length APP is also cleaved by  $\alpha$ -secretase leading to the formation of soluble APP $\alpha$  (sAPP $\alpha$ ), which is non-amyloidogenic<sup>11</sup>.

$A\beta$  production in brain is a target for AD therapy, with the potential for a disease modifying effect by reducing  $A\beta$  levels<sup>12</sup>. Several BACE1 inhibitors (BACEi) are being tested in human clinical trials, but the optimum level of BACE1 inhibition required for the treatment of AD remains to be determined<sup>13</sup>. A quantitative understanding of the effects of secretase inhibitors on the APP pathway may provide greater insights into dose-response pharmacology relationships.

Generally, measures of  $A\beta$  response in humans and primates can only be obtained in CSF and not in brain. However, it is believed that changes in  $A\beta$  concentrations in CSF reflect changes in brain  $A\beta$ <sup>14</sup>. Thus, CSF  $A\beta$  serves as key biomarker for  $A\beta$  production targeted therapies<sup>15</sup>. The cisterna magna ported (CMP) rhesus monkey model enables longitudinal sampling in the CSF outflow from the cisterna magna in conscious rhesus. As APP is completely homologous between human and rhesus, the CMP rhesus monkey model is used to study the effects of secretase inhibitors<sup>16,17,18</sup>.

Several studies on the pharmacokinetics (PK) and the pharmacodynamics (PD) of

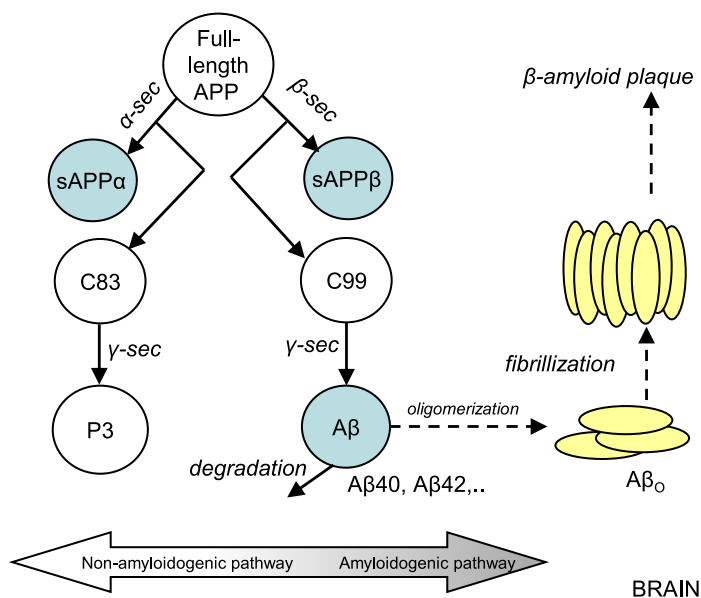


**Figure 3.1: Schematic representation of the amyloid hypothesis of AD.**

In the APP processing pathway, full length APP is cleaved by BACE1 ( $\beta$ -sec) or  $\alpha$ -secretase ( $\alpha$ -sec) to form sAPP $\beta$  and C99 or sAPP $\alpha$  and C83. C99 is then cleaved by  $\gamma$ -secretase ( $\gamma$ -sec) to form A $\beta$ . The amyloid hypothesis states that an imbalance in production and clearance of A $\beta$  can result in aggregation of A $\beta$ 42 fragments into amyloid plaque. *blue circles*: APP metabolites measured in CSF.

BACE1 and  $\gamma$ -secretase inhibitors have been reported<sup>19,14,20,21</sup>. Liu et al. 2013 proposed a mechanistic PK-PD model of BACE1 inhibition in monkeys. They identified the  $\beta$ -secretase cleavage step as the rate limiting step for A $\beta$  formation. However, their model is a simplification of the underlying system as no distinction is made between the  $\beta$ -secretase and  $\gamma$ -secretase cleavage steps and A $\beta$  was modelled as a direct product of APP. Potter et al. 2013 used compartmental modelling to investigate the APP processing pathway based on the results from a metabolic tracer study in humans with rare autosomal dominant AD (ADAD). A model with 18 compartments accounting for the kinetics of A $\beta$ 38, A $\beta$ 40 and A $\beta$ 42 enrichments, including compartments representing APP and C99 was proposed. However, the reported model is structurally and numerically unidentifiable, considering that not all APP metabolites were measured.

No systems pharmacology model has been reported that provides an integrated description of the effects of drugs on the APP metabolites. Systems pharmacology modelling is an extension of traditional mechanism-based PK-PD modelling, linking the system that

is affected by the drug to its treatment associated measured biomarkers. This involves computational analysis of the time course of the changes in biomarkers on the basis of a structural mathematical model that describes the underlying biological processes, while making a strict distinction between drug-specific and systems specific parameters. It has been demonstrated that such mechanism-based PK-PD models have much improved properties for extrapolation and prediction<sup>24,25</sup>. Systems pharmacology modelling will provide a quantitative understanding of the effects of drugs on the APP processing pathway to improve the prediction and magnitude of  $A\beta$  reducing effects.

The objective of this investigation was to characterize the multi-step production of  $A\beta$  in brain and its disposition into CSF in rhesus and obtain an indirect impression of  $A\beta_O$  using information from the monomeric  $A\beta$  species. To this end, CSF  $A\beta$  dynamic data from CMP monkeys treated with the BACEi MBI-5 were analysed. APP metabolites inter-relationships and their responses to MBI-5 were each measured by ELISA and metabolite responses were then integrated by means of a systems pharmacology modelling approach. Comprehensive, model-based information from MBI-5 PK and PD is integrated across time points, doses and endpoints, yielding information on dose response and APP metabolite (sAPP $\beta$ , sAPP $\alpha$  and  $A\beta$ ) responses and interrelationships. In this manner invaluable information is obtained on the functioning of the integrated biological system. The effect of BACE1 inhibition on  $A\beta_O$  is anticipated which will be measured in future studies.

## Materials and Methods

### Animals

Animal use procedures were conform to the Guide for the Care and Use of Laboratory Animals (Institute of Laboratory Animal Resources, National Research Council, 1996) and reviewed and approved by the Institutional Animal Care and Use Committee at Merck Research Laboratories. The CMP rhesus monkey model was described by<sup>17</sup>. The rhesus monkeys are chronically implanted with catheters in the cisterna magna, allowing repeated sampling of CSF and plasma in conscious rhesus. Six male animals, weighing between 5.2 and 11.7 kg (average, 8.7 kg), age 2 to 10 years (average, 8 years), were included in the study. These monkeys were captive-bred in a closed colony and individually housed.



### Drug administration and sampling

The study protocol and pharmacological profile of MBI-5 was described previously by Dobrowolska et al.<sup>26</sup>. The study protocol is summarized here. In a single dose, four-way, full crossover study, MBI-5 was administrated at 10, 30, 125 mg/kg (5 ml/kg), or vehicle (0.4% methylcellulose) p.o., with at least two weeks washout between each period. Plasma and CSF drug concentrations were collected at 0 (predose) and 3, 5, 7, 9, 13, 16, 19, 22, 25, 28, 31, 49, 55, 58, 73 and 145 h postdose, resulting in 17 plasma and CSF PK samples for each monkey per treatment group. 2 mL of blood and 1 mL of CSF were collected at each time point. The concentration of MBI-5 in the plasma and CSF samples was determined using LC-MS/MS.

The concentrations of A $\beta$ 40, A $\beta$ 42, sAPP $\alpha$  and sAPP $\beta$  were determined from CSF samples collected at -22, -20 and -1 h (predose) and 2, 4, 6, 8, 12, 15, 18, 21, 24, 27, 30, 48, 54, 57, 72 and 144 h postdose, giving 19 measurements of each biomarker for each monkey per treatment group. 1 mL of CSF were collected at each time point. The assays used for the concentration measurements were described previously<sup>27,28</sup>.

### PK-PD analysis

The PK-PD model was developed and fitted to the data by means of non-linear mixed effects modelling using the NONMEM software package version VI level 2<sup>29</sup>. This approach takes into account structural (fixed) effects and both intra- and interindividual variability. The following parameters are estimated: typical values of structural model parameters (population parameters, which define the average value for a parameter in a population) ( $\theta$ ), the variance and covariance of the interindividual variability ( $\omega^2$ ) and the variance of the residual error ( $\sigma^2$ ). A step-wise procedure was used to find the model that best fitted the data. A convergence criterion of three significant digits in the parameter estimates was used. The obtained minimum value of the objective function was used for the comparison of nested models. A decrease of 10.8 points in the minimum value of the objective function by adding an additional parameter, corresponding to  $p < 0.001$  in a  $\chi$ -squared distribution, was considered significant. The first-order conditional estimation approximation with  $\eta$ - $\epsilon$  interaction (FOCE interaction) was used for parameter estimation. Random effects at the individual level were included as exponential ( $e^{\eta}$ ), reflecting lognormal distributions of the individual model parameters:

$$\theta_i = \theta \times e^{(\eta_i)} \quad (3.1)$$

in which  $\theta_i$  is the value for the  $i^{\text{th}}$  individual;  $\theta$  is the typical value for the parameter, and  $\eta$  is an interindividual random effect, which is assumed to follow a normal distribution with mean zero and variance  $\omega^2$ .

The residual variability was explored with additive (Eq. 3.2) and proportional (Eq. 3.3) error models or a combination of both (Eq. 3.4) .

$$y_{ijk} = f(\theta_{ij}) + \epsilon_{ijk} \quad (3.2)$$

$$y_{ijk} = f(\theta_{ij}) \times (1 + \epsilon_{ijk}) \quad (3.3)$$

$$y_{ijk} = f(\theta_{ij}) \times (1 + \epsilon_{ijk1}) + \epsilon_{ijk2} \quad (3.4)$$

where  $y_{ijk}$  is the  $k^{\text{th}}$  observation on the  $j^{\text{th}}$  occasion for the  $i^{\text{th}}$  individual;  $f(\theta_{ij})$  is the corresponding model predicted observation and  $\epsilon$  represents the residual departure of the observed concentration from the predicted concentration, which is assumed to follow a normal distribution with mean zero and variance  $\sigma^2$ .

To evaluate the prediction of the central tendency and distribution of the observed data by the model a visual predictive check (VPC) was performed in which the median and the 90% inter-quantile range of the data simulated with the developed model were plotted together with the observations. A validated result would have close agreement of median observed and predicted line with  $\sim 90\%$  of the observations falling within the 90% prediction interval.

The NONMEM software package was implemented on an Intel QuadCore (Intel®Core™ i7 CPU860, 2.80 GHz, 3.24 GB RAM) and Compaq Visual Fortran (version 6.6, Compaq Computer Corporation, Houston, Texas, USA) was used as compiler. Data management and model assessment was done using the statistical software package S-PLUS for Windows (version 8.0 Professional, Insightful Corp., Seattle, USA).

### **Model description**

The systems pharmacology model of MBI-5 was developed by sequential analysis of PK and PD data. The PK model of MBI-5 was based on simultaneous analysis of plasma and CSF PK data. The results of the PK data analysis is provided in the Supplemental Material. The PK profiles of MBI-5 observed in plasma and CSF were adequately described by a three-compartmental model (Supplemental Figure S3.2) and the PK parameters were estimated with good precision (Supplemental Table S3.1), thus the model could serve as input for PD model analysis.

The biomarker response profiles of MBI-5 measured in CSF were adequately described

by a model containing compartments for five variables: APP, sAPP $\beta$ , sAPP $\alpha$ , A $\beta$ <sub>40</sub> and A $\beta$ <sub>42</sub> (Figure 3.2). The production of APP was believed to be zero order, i.e. a constant production of APP. It was assumed that there is no alternative proteolytic enzyme cleaving full length APP other than  $\alpha$ -secretase and BACE1. As both sAPP $\beta$  and C99 are products of APP cleavage by BACE1, sAPP $\beta$  and C99 were presumed to follow the same kinetics and therefore sAPP $\beta$  could be used in the model as surrogate precursor for A $\beta$ . The production of sAPP $\alpha$ , sAPP $\beta$  and A $\beta$  were assumed to be first order, i.e. dependent on the concentration of its precursor. The interaction between APP, sAPP $\beta$ , sAPP $\alpha$ , A $\beta$ <sub>40</sub> and A $\beta$ <sub>42</sub> is described by Eq. 3.5 - Eq. 3.9:

$$\frac{d}{dt}APP = Rin_{APP} - (Rin_{\beta} \times EFF + Rin_{\alpha}) \times APP \quad (3.5)$$

$$\frac{d}{dt}sAPP_{\alpha} = Rin_{\alpha} \times APP - Rout_a \times sAPP_{\alpha} \quad (3.6)$$

$$\frac{d}{dt}sAPP_{\beta} = Rin_{\beta} \times EFF \times APP - (Kin_{40} + Kin_{42}) \times sAPP_{\beta} \quad (3.7)$$

$$\frac{d}{dt}A_{\beta 40} = Kin_{40} \times sAPP_{\beta} - Kout \times A_{\beta 40} \quad (3.8)$$

$$\frac{d}{dt}A_{\beta 42} = Kin_{42} \times sAPP_{\beta} - Kout \times A_{\beta 42} \quad (3.9)$$

The rate of change of APP with respect to time in the presence of the inhibitor is described by Eq. 3.5, in which the BACE1 cleavage inhibition is incorporated by the factor *EFF*. *EFF* is the degree of inhibition caused by MBI-5, expressed as shown in Eq. 3.10.

$$EFF = 1 - \frac{C_{target}^{GAM} \times Imax}{C_{target}^{GAM} + IC50^{GAM}} \quad (3.10)$$

Where  $C_{target}$  is the target site concentration of MBI-5,  $IC50$  the  $C_{target}$  that results in 50% inhibition of BACE1,  $Imax$  is the maximum response and  $GAM$  is the Hill coefficient.  $C_{target}$  was derived from the PK model as:



$$C_{\text{target}} = C_{\text{plasma}} \times \frac{AUC_{\text{CSF}}}{AUC_{\text{plasma}}} \quad (3.11)$$

Where  $AUC_{\text{CSF}}$  and  $AUC_{\text{plasma}}$  are the areas under the CSF and plasma concentration time curves, respectively. Here,  $C_{\text{target}}$  is assumed to follow the same profile as  $C_{\text{plasma}}$ , but at a level between  $C_{\text{CSF}}$  and  $C_{\text{plasma}}$ .

It is assumed that the system is in steady state when no treatment is given ( $EFF=1$ ). At the treatment free-state, the change of the variables with respect to time is:

$$\frac{d}{dt}APP = 0 \quad \frac{d}{dt}sAPP\alpha = 0 \quad \frac{d}{dt}sAPP\beta = 0 \quad \frac{d}{dt}A\beta_{40} = 0 \quad \frac{d}{dt}A\beta_{42} = 0 \quad (3.12)$$

These steady state conditions were used to derive part of the system parameters. From Eq. 3.12 and Eq. 3.5 it follows that the source of APP ( $Rin_{APP}$ ) is:

$$Rin_{APP} = (Rin\alpha + Rin\beta) \times APP_{\text{base}} \quad (3.13)$$

Where  $APP_{\text{base}}$  is the baseline level of APP, which is assumed to be equal to the sum of the baseline levels of sAPP $\alpha$  and sAPP $\beta$ , as it was assumed that there is no alternative proteolytic enzyme cleaving full length APP other than  $\alpha$ -secretase and BACE1.

Using Eq. 3.12 and Eq. 3.6 the sAPP $\alpha$  formation rate ( $Rin\alpha$ ), equivalent to the  $\alpha$ -secretase cleavage step, can be derived:

$$Rin\alpha = Rout_a \times \frac{sAPP\alpha_{\text{base}}}{APP_{\text{base}}} \quad (3.14)$$

Where sAPP $\alpha_{\text{base}}$  is the baseline level of sAPP $\alpha$ .

The sAPP $\beta$  formation rate ( $Rin\beta$ ), equivalent to the BACE1 cleavage step, follows from Eq. 3.12 and Eq. 3.7:

$$Rin\beta = (Kin_{40} + Kin_{42}) \times \frac{sAPP\beta_{\text{base}}}{APP_{\text{base}}} \quad (3.15)$$

Where  $sAPP\beta_{base}$  is the baseline level of  $sAPP\beta$ .

From Eq. 3.12 and Eq. 3.8 the  $A\beta40$  formation rate ( $Kin40$ ), equivalent to a  $\gamma$ -secretase cleavage step can be calculated:

$$Kin_{40} = Kout \times \frac{A\beta40_{base}}{sAPP\beta_{base}} \quad (3.16)$$

Where  $A\beta40_{base}$  is the baseline level of  $A\beta40$ .  $sAPP\beta_{base}$  is the baseline level of  $sAPP\beta$ , used here as surrogate for the baseline level of  $C99$ .

From Eq. 3.9 and Eq. 3.12, with substitution of  $Kout$  from Eq.3.16, the  $A\beta42$  formation rate ( $Kin42$ ), equivalent to a  $\gamma$ -secretase cleavage step, is deduced:

$$Kin_{42} = Kin_{40} \times \frac{A\beta42_{base}}{A\beta40_{base}} \quad (3.17)$$

Where  $A\beta42_{base}$  is the baseline level of  $A\beta42$ .

The model structure includes four transit compartments (Fig. 3.2), one for each biomarker measured in CSF ( $sAPP\alpha$ ,  $sAPP\beta$ ,  $A\beta40$ ,  $A\beta42$ ), to account for transport from the target site in the brain to CSF. These transit processes are described, in general, by Eq. 3.18:

$$\frac{d}{dt} species_{CSF} = Kt \times (species - species_{CSF}) \quad (3.18)$$

Where  $Kt$  is the transit rate for the particular species ( $KtAP$  for  $sAPP\alpha$  and  $sAPP\beta$  and  $KtAB$  for  $A\beta40$  and  $A\beta42$ ).

The system defined above can now be extended to incorporate an  $A\beta_O$  pool for  $A\beta42$  oligomerization. The addition of the  $A\beta_O$  pool to the model structure requires adaptation of Eq. 3.9, describing  $A\beta42$  dynamics. The exchange between the  $A\beta_O$  pool and the  $A\beta42$  compartment is described by Eq. 3.19 and Eq. 3.20:

$$\frac{d}{dt} A\beta_{42} = Kin_{42} \times sAPP\beta - Kout_{42} \times A\beta_{42} - Kpl \times A\beta_{42} + Krev \times A\beta_O \quad (3.19)$$

$$\frac{d}{dt} A\beta_O = Kpl \times A\beta_{42} - Krev \times A\beta_O \quad (3.20)$$

Where  $K_{pl}$  and  $K_{rev}$  are the  $A\beta_{42}$  oligomerization and dissociation rate, respectively, which are dependent on the baseline values of  $A\beta_{42}$  and the  $A\beta_O$  pool ( $A\beta_{42_{base}}$  and  $A\beta_{O_{base}}$ , resp.) according to Eq. 3.21:

$$K_{rev} = \frac{K_{pl} \times A\beta_{42_{base}}}{A\beta_{O_{base}}} \quad (3.21)$$

## Results

### Separate empiric models described response of each APP metabolite

Initially, empirical PK-PD models were developed to quantify the exposure-response relationships for each CSF APP metabolite ( $A\beta_{40}$ ,  $A\beta_{42}$ ,  $sAPP\alpha$  and  $sAPP\beta$ ) of the BACEi MBI-5 in monkeys. The typical model structure of each APP metabolite-inhibitor combination consisted of a transit model with 1 or 2 compartments, with the drug effect modelled relative or subtractive to baseline using an  $I_{max}/E_{max}$  function. A summary overview of the results of these models is depicted in Table 3.1. The empirical models provided consistency of drug effects across APP metabolites (identified potencies  $A\beta_{40}$ : 0.0254  $\mu\text{M}$  (95% CI, 0.0246-0.0262);  $A\beta_{42}$ : 0.0455  $\mu\text{M}$  (95% CI, 0.0351-0.0559);  $sAPP\beta$ : 0.0490  $\mu\text{M}$  (95% CI, 0.0192-0.0788);  $sAPP\alpha$ : 0.0265  $\mu\text{M}$  (95% CI, 0.0135-0.0395)). The mean transit time through the compartments of the models was lower for  $A\beta_{40}$  and  $A\beta_{42}$  than for  $sAPP\beta$  and  $sAPP\alpha$ . This indicates that the response of  $A\beta_{40}$  and  $A\beta_{42}$  will appear earlier in CSF, even though  $sAPP\beta$  is a sequentially earlier product of the amyloidogenic APP pathway.

### A systems model to describe APP metabolite responses

A comprehensive compartmental PK-PD model, incorporating MBI-5 PK and CSF APP metabolites ( $A\beta_{40}$ ,  $A\beta_{42}$ ,  $sAPP\alpha$  and  $sAPP\beta$ ) concentrations was developed to quantify APP metabolite responses to BACE1 inhibition in monkeys. The model is schematically presented in Figure 3.2. The model described production, elimination, and brain-to-CSF transport of each APP metabolite, as well as their interrelationships (Figure 3.7). The rate of APP metabolism was assumed to be close to the maximal capacity of the enzymes involved<sup>30</sup>. Thus, APP production was approximated to follow zero-order kinetics.  $sAPP\beta$  was used in the model structure as a surrogate substrate for C99 in the



**Table 3.1: Summary parameters of the separate empiric model fits for each APP metabolite**

| PARAMETER                          | DESCRIPTION   | UNIT    | APP METABOLITE    |                |                |                   |
|------------------------------------|---|---------|-------------------|----------------|----------------|-------------------|
|                                    |   |         | A $\beta$ 40      | A $\beta$ 42   | sAPP $\alpha$  | sAPP $\beta$      |
| baseline                           | Baseline  | pM      | 722               | 24.8           | 1040           | 1190              |
| IM/EM                              | Baximal inhibition / effect                                 |         | 100% <sup>a</sup> | 20.4 pM        | 167%           | 100% <sup>a</sup> |
| IC <sub>50</sub> /EC <sub>50</sub> | median inhibition / effect concentration                    | $\mu$ M | 0.0254            | 0.0455         | 0.0265         | 0.0490            |
| CV                                 | Coefficient of variation IC <sub>50</sub> /EC <sub>50</sub> | %       | 1.63              | 11.6           | 25.0           | 31.0              |
| GAM                                | Hill coefficient  |         | 1 <sup>a</sup>    | 1 <sup>a</sup> | 1 <sup>a</sup> | 1 <sup>a</sup>    |
| MTT <sup>b</sup>                   | Mean transit time   | h       | 5.155             | 3.597          | 15.873         | 19.417            |

<sup>a</sup> Fixed.

<sup>b</sup>  $MTT = \frac{1}{Kt} \times (n + 1)$ , where  $n$  is the number of transit compartments and  $Kt$  is the transit rate.

$\gamma$ -secretase cleavage step. As both sAPP $\beta$  and C99 are products of the APP cleavage by BACE1, their formation rates should be the same and thus use of sAPP $\beta$  as a surrogate for C99 was justified. To account for transport from the target site in the brain to CSF, the model included one transit compartment for each APP metabolite. The drug effect was incorporated in the model as the inhibition of loss of the APP precursor pool, equivalent to the BACE1 cleavage step.

### **MBi-5 increased sAPP $\alpha$ and decreased sAPP $\beta$ and A $\beta$ in a dose dependent manner**

APP metabolite CSF concentrations showed a dose-dependent response in the presence of the BACEi. The dose-dependent increase of sAPP $\alpha$  and the corresponding decreases of sAPP $\beta$  and A $\beta$  were described by the model with a single drug effect. A potency (IC<sub>50</sub>) of 0.0256  $\mu$ M (95% CI, 0.0137-0.0375) was identified. This value is close to the *in vitro* inhibition constant ( $Ki$ ) of 10 nM for MBi-5 inhibition of purified BACE1 and also close to the IC<sub>50</sub> for inhibition of A $\beta$  production in intact cells of 24 $\pm$ 6 nM<sup>26</sup>. When estimated, the maximal inhibition (Imax) was close to 1. Therefore Imax could be fixed to 1, indicating 100% inhibition of BACE1 at sufficient high drug concentrations. Figures 3.3 to 3.6 show the model description of each APP metabolite for each dose group.

### **A $\beta$ <sub>O</sub> pool required to account for differential effect on A $\beta$ 40 and A $\beta$ 42**

A differential effect of BACE1 inhibition was observed for A $\beta$ 40 and A $\beta$ 42: a higher response is observed in the data for A $\beta$ 40 than for A $\beta$ 42 (e.g. Figure 3.6E and 3.6G). This differential effect could be described by extending the model with an A $\beta$ <sub>O</sub> pool connected to the A $\beta$ 42 compartment, resulting in an adequate description of sAPP $\beta$ , sAPP $\alpha$ , A $\beta$ 40

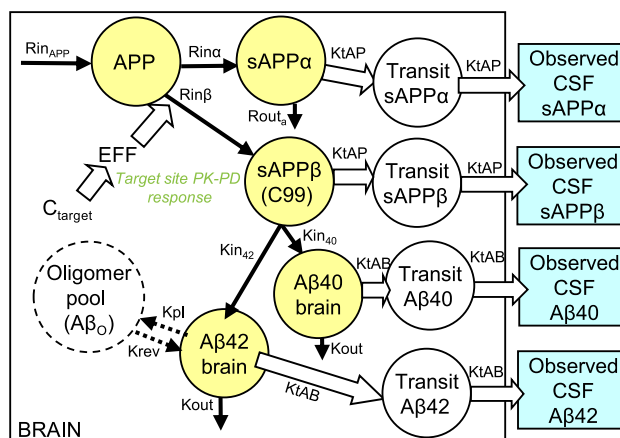


**Figure 3.2: Schematic of systems model of APP processing.**

The model comprised nine compartments: Five biomarker compartments in brain (yellow circles) and four transit compartments from brain to CSF (white circles). Four biomarkers were measured in CSF (sAPP $\alpha$ , sAPP $\beta$ , A $\beta$ 40 and A $\beta$ 42), indicated by the blue boxes. The extended model included additionally an A $\beta$ <sub>O</sub> compartment (dashed circle). The drug effect (EFF) inhibited Rin $\beta$ . As driver of biomarker response  $C_{\text{target}}$  was used, which was derived from the PK model (see Supplemental Material). sAPP $\beta$  was used in the model structure as a surrogate substrate of C99 in the  $\gamma$ -secretase cleavage step.

APP: A $\beta$ -precursor protein; A $\beta$ : amyloid- $\beta$ -peptide;  $C_{\text{target}}$ : drug concentration target site;  $Kin_{40}$ : A $\beta$ 40 formation rate;  $Kin_{42}$ : A $\beta$ 42 formation rate;  $Kout$ : A $\beta$  degradation rate;  $Kpl$ : Oligomerization rate;  $Krev$ : A $\beta$ <sub>O</sub> dissociation rate;  $KtAB$ : transit rate A $\beta$  from brain to CSF;  $KtAP$ : transit rate sAPP $\alpha$  and sAPP $\beta$  from brain to CSF;  $RinAPP$ : zero order input constant for APP;  $Rin\alpha$ : sAPP $\alpha$  formation rate;  $Rin\beta$ : sAPP $\beta$  formation rate;  $Rout$ : sAPP $\beta$  degradation rate;  $Rout\alpha$ : sAPP $\alpha$  degradation rate.

and A $\beta$ 42 CSF concentration time profiles for each dose group (Figures 3.3, 3.4, 3.5 and 3.6, respectively). Incorporating the A $\beta$ <sub>O</sub> pool in the model improved the description of A $\beta$ 40 response for the 30 and 125 mg/kg dose group (compare Figure 3.5E to Figure 3.5F and Figure 3.6E to Figure 3.6F), as well as the description of the 125 mg/kg dose for A $\beta$ 42 response (compare Figure 3.6G to Figure 3.6H). Furthermore, the description of sAPP $\beta$  response for 125 mg/kg dose (compare Figure 3.6C to Figure 3.6D) was improved. Exchange of an A $\beta$ 40 monomer pool with an A $\beta$ <sub>O</sub> pool was evaluated, but could not be identified.

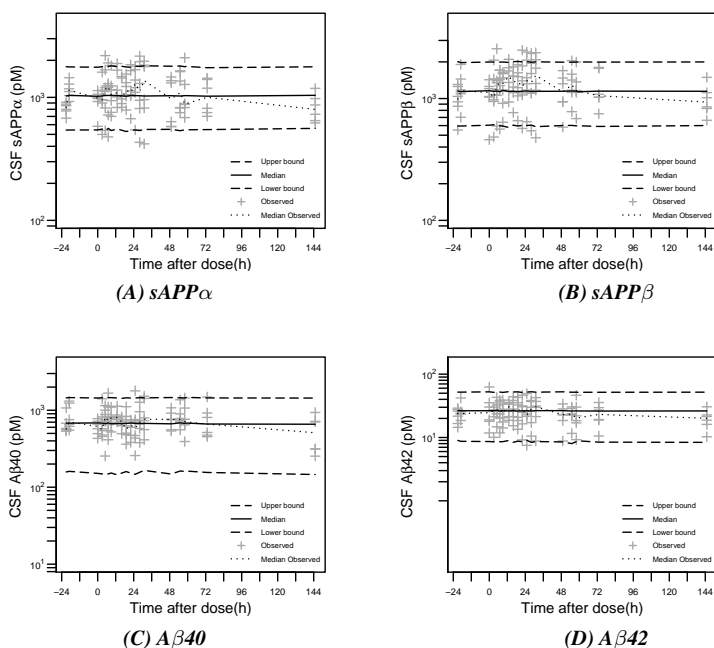


**Figure 3.3: Placebo. Visual predictive check of biomarker response vs. time profile of placebo in the rhesus with 90% confidence interval.** Predictions were performed with model without  $A\beta_O$  compartment ((A), (B), (C), (D)). Predictions performed with model with  $A\beta_O$  pool had identical results (not shown). Observation sample size:  $n=114$  for each APP metabolite from 6 monkeys collected over 7 days.

Plus-symbols represent observed measurements. Dotted line corresponds to the median observed profile. Solid lines show the median simulated profiles. The long-dashed lines correspond to the 90% prediction intervals obtained from 1000 individual simulated profiles.



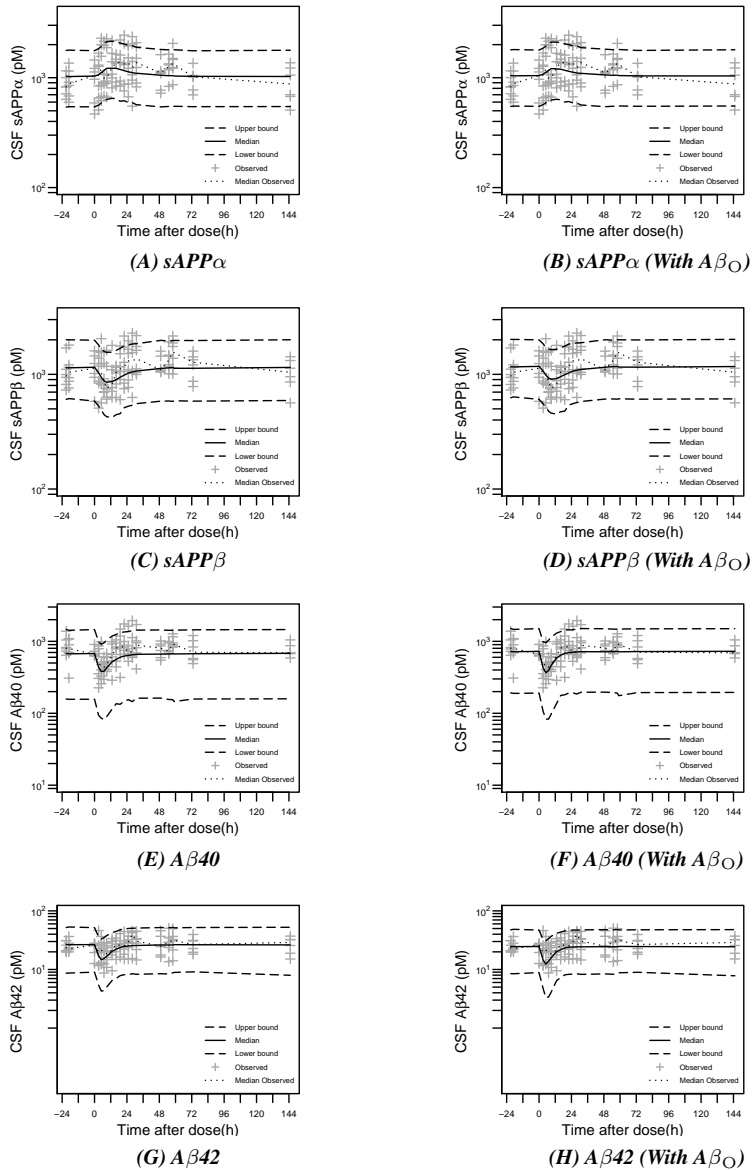


**Figure 3.4: Dose 10 mg/kg. Visual predictive check of biomarker response vs. time profile of MBI-5 in the rhesus with 90% confidence interval.** Predictions were performed with model with ((B), (D), (F), (H)) and without ((A), (C), (E), (G))  $A\beta_O$  compartment. Observation sample size:  $n=114$  for each APP metabolite from 6 monkeys collected over 7 days. Plus-symbols represent observed measurements. Dotted line corresponds to the median observed profile. Solid lines show the median simulated profiles. The long-dashed lines correspond to the 90% prediction intervals obtained from 1000 individual simulated profiles.

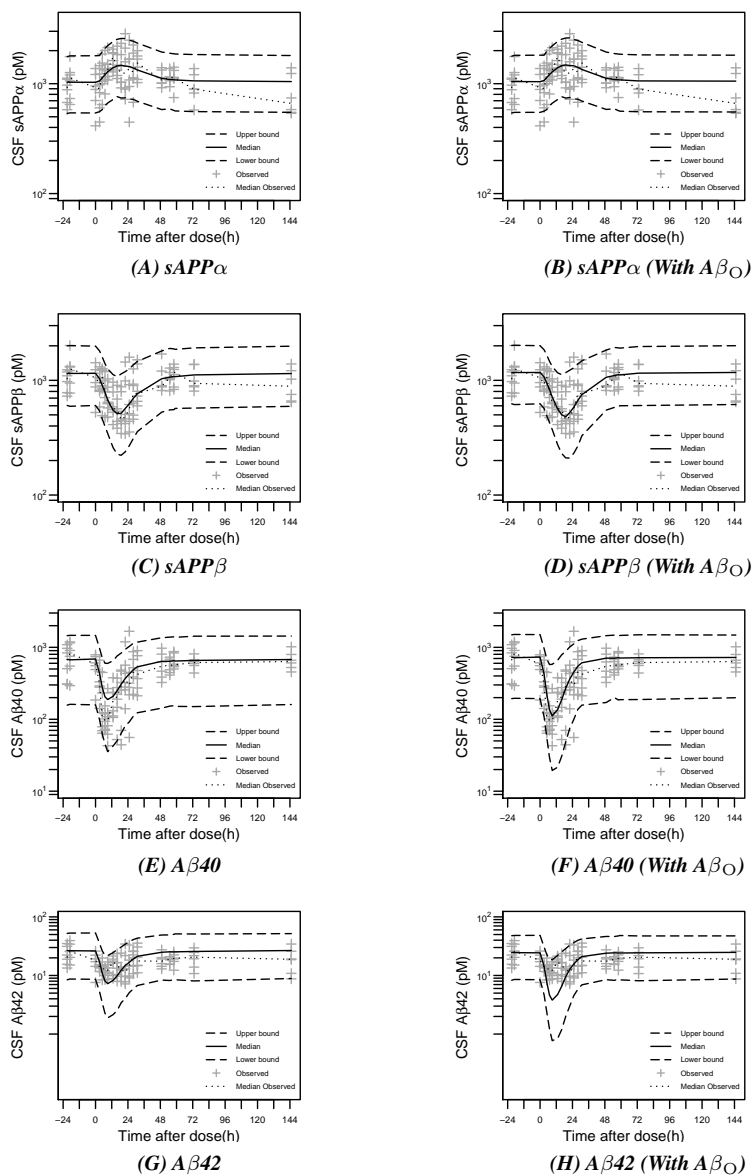


**Figure 3.5: Dose 30 mg/kg. Visual predictive check of biomarker response vs. time profile of MBI-5 in the rhesus with 90% confidence interval.** Predictions were performed with model with ((B), (D), (F), (H)) and without ((A), (C), (E), (G))  $A\beta_O$  compartment. Observation sample size:  $n=114$  for each APP metabolite from 6 monkeys collected over 7 days. Plus-symbols represent observed measurements. Dotted line corresponds to the median observed profile. Solid lines show the median simulated profiles. The long-dashed lines correspond to the 90% prediction intervals obtained from 1000 individual simulated profiles.

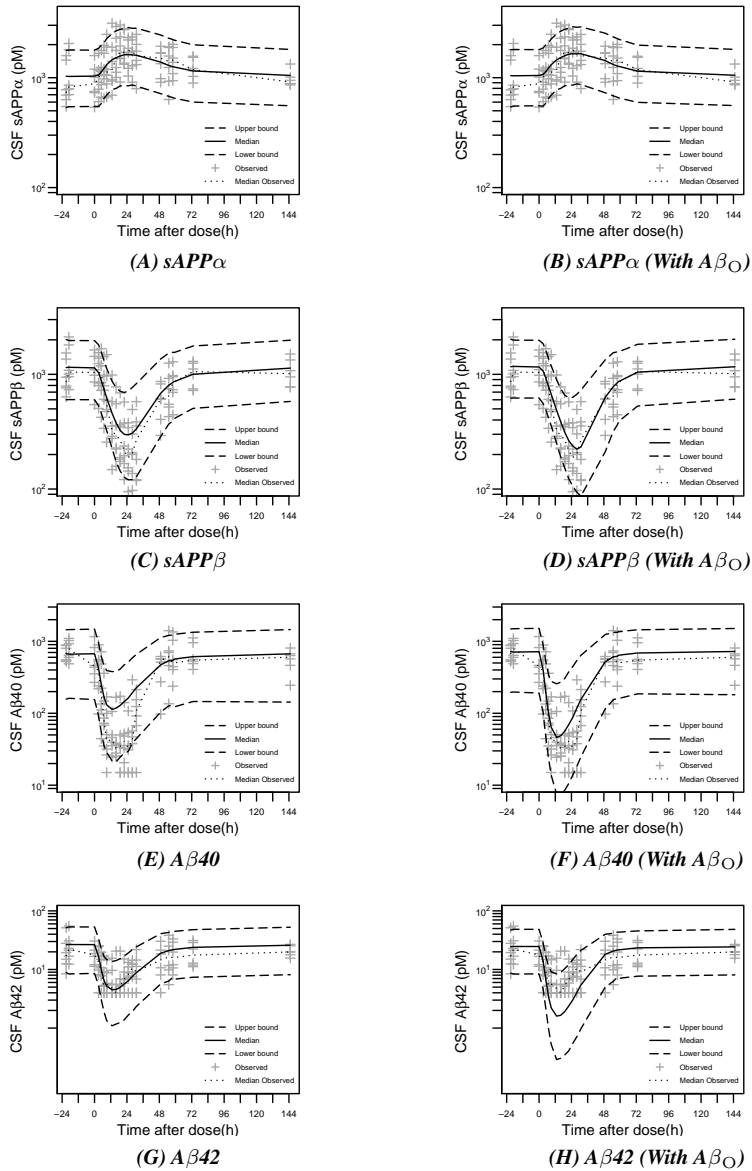


**Figure 3.6: Dose 125 mg/kg. Visual predictive check of biomarker response vs. time profile of MBI-5 in the rhesus with 90% confidence interval.** Predictions were performed with model with ( (B), (D), (F), (H)) and without ( (A), (C), (E), (G))  $A\beta_O$  compartment. Observation sample size:  $n=114$  for each APP metabolite from 6 monkeys collected over 7 days. Plus-symbols represent observed measurements. Dotted line corresponds to the median observed profile. Solid lines show the median simulated profiles. The long-dashed lines correspond to the 90% prediction intervals obtained from 1000 individual simulated profiles.

### Model parameters

The population parameters and intra- and interanimal variability were optimized for the study population and are depicted in Table 3.2. A sequence of models with interanimal variability on different parameters was tested and the results compared, in order to select the best random effects model structure. The final model included interanimal variability for the baseline of sAPP $\beta$  and the IC<sub>50</sub> of MBI-5. Both were included as exponential in nature, reflecting lognormal distributions of the individual model parameters. As the baselines of the other APP metabolites were modelled as function of the baseline of sAPP $\beta$ , its interanimal variability reflects also on the other baselines. Residual variability was included for each APP metabolite (sAPP $\beta$ , sAPP $\alpha$ , A $\beta$ 40, A $\beta$ 42), as proportional error models, assuming that the residual errors are normally distributed. The identified residual variability was higher for A $\beta$ 40 and A $\beta$ 42 than for sAPP $\beta$  and sAPP $\alpha$ . System specific parameters could be distinguished from drug specific parameters (all correlations <0.95).

Incorporating the A $\beta$ <sub>O</sub> pool in the model improved the description and did not affect the parameter estimate of the IC<sub>50</sub> significantly: With A $\beta$ <sub>O</sub> pool an IC<sub>50</sub> of 0.0269  $\mu$ M (95% CI, 0.0154-0.0384) was identified and without A $\beta$ <sub>O</sub> pool the IC<sub>50</sub> was 0.0256  $\mu$ M (95% CI, 0.0137-0.0375). The incorporation of the A $\beta$ <sub>O</sub> pool affected the Hill coefficient of the sigmoidal I<sub>max</sub> concentration response relationship. The A $\beta$ <sub>O</sub> pool resulted in a Hill coefficient slightly deviating from unity: With the A $\beta$ <sub>O</sub> pool a Hill coefficient of 1.53 (95% CI, 1.14-1.92) was identified and without A $\beta$ <sub>O</sub> pool the Hill coefficient was 1 (fixed). This mainly improved the description of the APP metabolite concentration response curves for the higher dose groups (Figure 3.6).

### Higher brain-to-CSF transport of A $\beta$

It was not possible to separate the rate of the  $\gamma$ -secretase cleavage from the brain-to-CSF transport. The transit rate for A $\beta$ 40 and A $\beta$ 42 was assumed to be equal and fast. Therefore, the transit rate from brain to CSF for A $\beta$ 40 and A $\beta$ 42 was fixed to an arbitrary high value (10 h<sup>-1</sup>). Then, the A $\beta$  half-life of 0.7 h reflects delays due to the  $\gamma$ -secretase cleavage step and brain-to-CSF transfer. For sAPP $\beta$  and sAPP $\alpha$  the transit rate was estimated to be 0.0985 h<sup>-1</sup>. This value should be interpreted relative to the A $\beta$  transit from brain-to-CSF. For sAPP $\alpha$  the brain-turnover (0.8 h) could be distinguished from the half-life of brain-to-CSF transfer (7.0 h). A $\beta$  is transported from brain to CSF approximately 10<sup>2</sup>-fold faster than sAPP $\alpha$ . As a result, the response of A $\beta$  to drug treatment will appear earlier in CSF than the response of sAPP $\alpha$ , even though sAPP $\alpha$  is a sequentially earlier product of the



**Table 3.2: Population parameter estimates including coefficient of variation (CV%) for the extended model with  $A\beta_O$  pool**

| PARAMETER                      | DESCRIPTION   | VALUE              | UNIT     | CV%  |
|--------------------------------|---|--------------------|----------|------|
| <i>Structural parameters</i>   |   |                    |          |      |
| $sAPP\beta_{base}$             | baseline $sAPP\beta$                                    | $1.19 \times 10^3$ | pM       | 11.6 |
| $Fbase_{A\beta40}^b$           | $A\beta40$ baseline as fraction of $sAPP\beta_{base}$   | 0.611              |          | 12.3 |
| $Fbase_{A\beta42}^c$           | $A\beta42$ baseline as fraction of $sAPP\beta_{base}$   | 0.0210             |          | 8.38 |
| $Fbase_{sAPP\alpha}^d$         | $sAPP\alpha$ baseline as fraction of $sAPP\beta_{base}$ | 0.894              |          | 2.84 |
| Kout                           | degradation rate $A\beta40$ and $A\beta42$              | 0.940              | $h^{-1}$ | 13.6 |
| Rout <sub>a</sub>              | degradation rate $sAPP\alpha$                           | 0.856              | $h^{-1}$ | 30.8 |
| KtAP                           | transit rate $sAPP\alpha$ and $sAPP\beta$               | 0.0985             | $h^{-1}$ | 2.82 |
| KtAB <sup>a</sup>              | transit rate $A\beta$                                   | 10                 | $h^{-1}$ |      |
| IM <sup>a</sup>                | maximal inhibition (Imax)                               | 1                  |          |      |
| IC <sub>50</sub>               | median inhibition concentration                         | 0.0269             | $\mu M$  | 21.8 |
| GAM                            | Hill coefficient  | 1.53               |          | 13.1 |
| Kpl                            | oligomerization rate                                    | 0.524              | $h^{-1}$ | 20.0 |
| $A\beta_O_{base}$              | baseline $A\beta_O$                                     | 278                | pM       | 41.0 |
| <i>Interanimal variability</i> |   |                    |          |      |
| $\omega^2_{BSAPb}^e$           | Interanimal variability $sAPP\beta$ baseline            | 0.0568             |          | 30.1 |
| $\omega^2_{IC50}^e$            | Interanimal variability IC50                            | 0.279              |          | 35.5 |
| <i>Residual error</i>          |   |                    |          |      |
| $\sigma^2_{A\beta40}^f$        | Residual variability $A\beta40$                         | 0.240              |          | 12.7 |
| $\sigma^2_{A\beta42}^f$        | Residual variability $A\beta42$                         | 0.161              |          | 12.4 |
| $\sigma^2_{sAPP\beta}^f$       | Residual analysed $sAPP\beta$                           | 0.0621             |          | 23.5 |
| $\sigma^2_{sAPP\alpha}^f$      | Residual variability $sAPP\alpha$                       | 0.0634             |          | 10.6 |

<sup>a</sup> Fixed.<sup>b</sup>  $A\beta40_{base} = Fbase_{A\beta40} \times sAPP\beta_{base}$ .<sup>c</sup>  $A\beta42_{base} = Fbase_{A\beta42} \times sAPP\beta_{base}$ .<sup>d</sup>  $sAPP\alpha_{base} = Fbase_{sAPP\alpha} \times sAPP\beta_{base}$ .<sup>e</sup> Interanimal variability is assumed to follow a normal distribution with mean zero and variance  $\omega^2$ .<sup>f</sup> Residual variability is assumed to follow a normal distribution with mean zero and variance  $\sigma^2$ .

### APP pathway.

It was not possible to identify the brain-turnover of  $sAPP\beta$  as a separate parameter. In the model structure,  $sAPP\beta$  was used as a surrogate substrate for C99 in the  $\gamma$ -secretase cleavage step, driving the response of  $A\beta$ . Therefore, the  $\gamma$ -secretase cleavage step could not be separated from  $sAPP\beta$  elimination.

### APP metabolites interrelationships

The proteolytic cleavage rates of APP through the action of BACE1 ( $Rin\beta$ ) and  $\alpha$ -secretase ( $Rin\alpha$ ) were calculated from the model parameters according to Eq. 5.12 and Eq. 5.11 to be  $0.314 h^{-1}$  and  $0.404 h^{-1}$  indicating that 56% of full length APP is cleaved

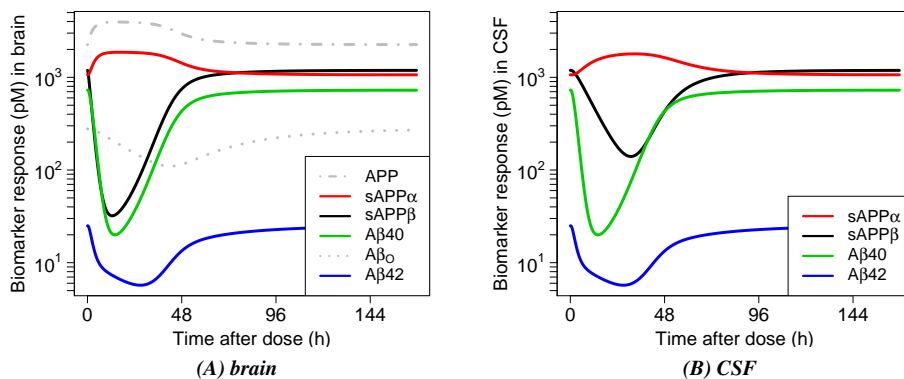


**Figure 3.7: Graphical insight into the biomarker responses in brain and CSF, using the identified systems model of the APP processing pathway.**

The biomarker responses in brain and CSF are predicted after a single dose of 125 mg MBI-5, using the typical parameter estimates.

APP grey dotted line; sAPP $\alpha$  red solid line; sAPP $\beta$  black solid line; A $\beta$ <sub>40</sub> green solid line; A $\beta$ <sub>O</sub> grey dotted line; A $\beta$ <sub>42</sub> blue solid line.

by  $\alpha$ -secretase and 44% by BACE1. The formation rates of A $\beta$ <sub>40</sub> and A $\beta$ <sub>42</sub> were calculated according to S4.27 and 5.15. The higher  $Kin_{40}$  ( $0.574 \text{ h}^{-1}$ ) than  $Kin_{42}$  ( $0.020 \text{ h}^{-1}$ ) is in line with previously reported findings of the ratio between A $\beta$ <sub>42</sub> and A $\beta$ <sub>40</sub> of about 1:10 in non-Alzheimer brain<sup>31</sup>. A difference in A $\beta$ <sub>40</sub> and A $\beta$ <sub>42</sub> degradation rate ( $Kout$ ) was also evaluated during the model development process, but this could not adequately capture the response profile of A $\beta$ <sub>42</sub>.

The developed model could be used to predict biomarker interrelationships in response to BACE1 inhibition and visualize the response of APP and A $\beta$ <sub>O</sub> (3.7A) in brain. APP increases after BACE1 inhibition and appears to be shunted down the  $\alpha$ -secretase pathway, resulting in an increase of sAPP $\alpha$  product. The elevation in sAPP $\alpha$  in the data drives the modelling conclusion that there is some increase in APP in the setting of BACE1 inhibition but it is fairly modest. The A $\beta$ <sub>O</sub> level decreases after BACE1 inhibition, indicating that there is reduced formation of A $\beta$ <sub>O</sub> by reduced levels of monomeric A $\beta$ <sub>42</sub> and that A $\beta$ <sub>O</sub> dissociates to monomeric A $\beta$ <sub>42</sub>. The latter influences the shape of the A $\beta$ <sub>42</sub> response curve, which is different than the shape of the A $\beta$ <sub>40</sub> response curve.

For sAPP $\beta$ , sAPP $\alpha$ , A $\beta$ <sub>40</sub> and A $\beta$ <sub>42</sub> the time courses of brain *versus* CSF responses were predicted (Figure 3.7A and 3.7B, respectively), showing that the earlier appearance of A $\beta$  response in CSF relative to sAPP $\alpha$  and sAPP $\beta$  arises from the slower brain to CSF transfer.

## Discussion

A systems model of the APP processing pathway was developed describing the interrelationships of  $A\beta_{40}$ ,  $A\beta_{42}$ ,  $sAPP\alpha$ , and  $sAPP\beta$  upon inhibition of BACE1 with MBI-5. All four APP metabolites provided consistent information regarding drug potency. The MBI-5 concentration-dependent decrease of the APP metabolites could be described by incorporating a single drug effect in the model: inhibition of the formation rate of  $sAPP\beta$ , equivalent to the BACE1 cleavage step. The model supported the notion that MBI-5 can provide 100% inhibition of BACE1, consistent with a complete blockage of  $A\beta$  production at high drug concentrations. The fact that MBI-5 can provide 100% inhibition of BACE1, implies that there are no inherent mechanistic limitations of the APP pathway to blocking  $A\beta$  production. Therefore, reaching complete inhibition largely depends on drug properties such as having sufficient potency, bioavailability and tolerability.

The relatively large interanimal variability identified on the baseline level of  $sAPP\beta$  (also reflecting on the baseline levels of the other APP metabolites) and the  $IC_{50}$  probably denotes the large intrinsic biological differences in APP processing between subjects. Residual variability was higher for  $A\beta_{40}$  and  $A\beta_{42}$  than for  $sAPP\beta$  and  $sAPP\alpha$ . Residual variability represents the uncertainty in the relationship between the concentrations predicted by the model and the observed concentration and includes any model misspecification error. The higher residual variability for  $A\beta$  could be related to the second cleavage step by  $\gamma$ -secretase, yielding  $A\beta$ . In the current analysis, no direct information was available regarding the  $\gamma$ -secretase cleavage step. This would require data from a  $\gamma$ -secretase inhibitor study. Such data may explain some of the residual variability identified for  $A\beta$ .

The systems model identified a higher brain-to-CSF transport of  $A\beta$  compared to  $sAPP\alpha$ . This results is consistent with the identified lower mean transit time for  $A\beta_{40}$  and  $A\beta_{42}$  compared to  $sAPP\alpha$  in the separate empirical models for each APP metabolite. The potencies identified in the empirical models were consistent with the single potency of  $0.0256 \mu\text{M}$  (95% CI, 0.0137-0.0375) identified using the systems model.

In the systems model, the APP production was approximated to follow zero-order kinetics. In reality, APP production is regulated by various factors, above all the synaptic activity<sup>32</sup>. In the current analysis, no quantitative data on the factors involved in APP production was available. It was assumed that the APP production was close to the maximum. Consequently, subtle changes in APP regulation would have little impact on APP metabolites formation.

Our modelling results imply that 56% of full length APP is cleaved by  $\alpha$ -secretase and 44% by BACE1. There is no quantitative data available from literature on the ratio of APP moving down the  $\alpha$ -secretase pathway and BACE1 pathway. Dobrowska et al. (2014) compared sAPP $\alpha$  and sAPP $\beta$  levels in human CSF from the lumbar region from cognitively normal and AD participants<sup>33</sup>. They identified a sAPP $\beta$ /sAPP $\alpha$  ratio of 0.59  $\pm$  0.4 (n=15) in cognitively normal healthy controls. Wu et al. (2011) reported sAPP $\alpha$  and sAPP $\beta$  levels in human brain cortex samples from elderly subjects without AD (n=16) of 37.1 pmol/g and 50.8 pmol/g, respectively<sup>27</sup>, resulting in a ratio of 0.73. However, both ratios do not directly reflect the ratio of APP cleaved by  $\alpha$ -secretase and BACE1, as the steady state sAPP $\beta$  and sAPP $\alpha$  levels in brain are the result of multiple processes such as production, degradation and transfer from brain-to-CSF. Levels in CSF are also affected by transfer through the lumbar region. In the current analysis, the developed model facilitated the separation of the different processes involved.

The systems analysis points to a difference in biology of A $\beta$ 40 and A $\beta$ 42. Firstly, a lower formation rate for A $\beta$ 42 than for A $\beta$ 40 was identified. This is consistent with the composition of A $\beta$  species reported for human CSF where the A $\beta$ 40 is the dominant isoform<sup>34</sup>. The relative production of A $\beta$ 40 and A $\beta$ 42 is probably regulated through changes in the  $\gamma$ -secretase cleavage site<sup>35,34</sup>. Secondly, the model included an A $\beta$ <sub>O</sub> pool in brain for A $\beta$ 42 but not A $\beta$ 40. Inclusion of exchange of an A $\beta$ 42 monomer pool with an A $\beta$ <sub>O</sub> pool could account for the differential effect of MBI-5 on A $\beta$ 40 and A $\beta$ 42 response observed in the data, in which the response for A $\beta$ 40 was higher than for A $\beta$ 42. Without incorporation of the A $\beta$ <sub>O</sub> pool in the model, the A $\beta$ 40 and A $\beta$ 42 response could not both be described adequately by a single drug effect. The identification of this A $\beta$ <sub>O</sub> constitutes the scientific basis for the identification of BACE1 inhibitor effects on higher ordered amyloid species. Due to the dissociation of A $\beta$ 42 oligomers to A $\beta$ 42 monomers during BACE1 inhibition the response for A $\beta$ 42 was lower than for A $\beta$ 40. The differential effect of the A $\beta$ <sub>O</sub> pool on A $\beta$ 42 is consistent with the biology of oligomer- and plaque formation where A $\beta$ 42 plays a more significant role than A $\beta$ 40<sup>1</sup>. A $\beta$ 42 is the major constituent of plaque and other species such as oligomers<sup>31,36</sup>.

The baseline level of the A $\beta$ <sub>O</sub> pool estimated by the model of 278 pM (1,255 pg/mL) should be interpreted as the level of A $\beta$ 42 monomers that is incorporated in the 'oligomer soup' in the brain, i.e. A $\beta$  dimers, trimers and high molecular weight species<sup>3</sup>. Here, no distinction is made between oligomeric species, as the A $\beta$ <sub>O</sub> pool is modelled as a pool in equilibrium with monomeric A $\beta$ 42 without correction for the number of subunits in multimeric species comprising the A $\beta$ <sub>O</sub> pool.

The  $A\beta_O$  dissociation rate ( $K_{rev}$ ) of  $1.308 \times 10^{-5} \text{ s}^{-1}$  identified here is relatively slow compared to the dissociation of  $A\beta$  aggregates acquired from *in vitro* analysis techniques. Gruning et al. (2013) detected the appearance of monomers from  $A\beta_{42}$  and  $A\beta_{40}$  protofibrils: the dissociation rate was  $1.4 \times 10^{-4}$  and  $1.2 \times 10^{-4} \text{ s}^{-1}$  for  $A\beta_{42}$  and  $A\beta_{40}$ , respectively. Narayan et al. (2012) reported  $A\beta_{40}$  fibrils releasing soluble  $A\beta_{40}$  species at a rate of  $9.3 \times 10^{-5} \text{ s}^{-1}$ . Sánchez et al. (2011) identified  $A\beta$  monomer off-rates of  $0.6 \times 10^{-2}$  and  $1.0 \times 10^{-2} \text{ s}^{-1}$  for  $A\beta_{40}$  and  $A\beta_{42}$  fibrils. It is difficult to compare rates obtained *in vivo* to those determined using *in vitro* approaches, as the *in vitro* experimental settings can have major impact. Moreover, the comparability of the dissociation rates to the value obtained in the current analysis is limited, because no particular oligomeric species was characterized in the systems pharmacology approach.

Quantitative measurements of the response of  $A\beta_O$  to drugs targeting the APP pathway, such as BACE1 inhibition, is of interest. Initial results of a new sensitive  $A\beta$  oligomer assay<sup>5</sup> suggest an  $A\beta_O$  baseline level of  $\sim 1.5 \text{ pg/mL}$  in rhesus CSF from the cisterna magna, which constitutes different oligomeric species (Mary Savage, Juliya Kalinina, unpublished observations). This number cannot be compared directly to the model derived  $A\beta_O$  baseline of  $1,255 \text{ pg/mL}$  representing  $A\beta$  subunits in the 'oligomer soup' in the brain. Also, the  $A\beta$ -oligomer assay may not pick up all oligomeric species or  $A\beta_O$  may dissociate to monomers during sample preparation. Furthermore, it remains to be seen if CSF  $A\beta_O$  measurements accurately reflect the brain  $A\beta_O$  concentrations<sup>40</sup>. The hydrophobicity of oligomers may make them very low or absent in aqueous fluids as CSF<sup>8</sup>. Recent data suggest that human CSF  $A\beta_O$  range between  $0.1$  and  $10 \text{ pg/mL}$  and human brain  $A\beta_O$  levels are  $252 \text{ pg/mL}$  in AD and  $87 \text{ pg/mL}$  in control brain<sup>5</sup>. Other data suggest 1,000-fold higher concentrations of  $A\beta_O$  than monomers in the soluble fraction of human AD cerebral cortex<sup>8</sup>. Relative concentrations in CSF will not necessarily reflect the relative concentrations in brain as oligomers are likely cleared to CSF much more slowly than monomeric  $A\beta$ . Additional dose-ranging studies of BACE1 inhibition in rhesus in which  $A\beta_O$  response is quantified, are ongoing. It is anticipated that including such data in the systems pharmacology model analysis will elucidate the relationship between the  $A\beta_O$  pool in the model and measurements of  $A\beta_O$ .

The identified  $A\beta_O$  pool should be interpreted with caution as an  $A\beta_O$  pool in rhesus may differ from an  $A\beta_O$  pool in AD patients with plaque burden. Rhesus do not develop dementia and neurodegenerative changes that characterize AD<sup>41</sup>. It is almost certain that the rhesus used in this study had far less amyloid deposition than a human AD patient. Therefore, the most crucial question is the nature of the identified  $A\beta_O$  pool in rhesus and

its pathological relevance to AD in human.  $A\beta$  oligomerization is a separate aggregation event. Certain oligomers are off-pathway species that do not further aggregate to amyloid fibrils. Coexistence of several oligomeric populations that do or do not propagate into fibrils is possible. If it can be demonstrated that there is a relationship between the soluble  $A\beta_O$  identified in rhesus and the AD brain-derived soluble  $A\beta_O$  and this could be correlated with neurotoxicity, then the relevance of  $A\beta_O$  in rhesus would be indisputable.

The lack of success of clinical trials targeting the APP pathway has been ascribed to the failure to reduce the level of toxic  $A\beta_O$ <sup>40</sup>. Plaques, toxic  $A\beta_O$  and  $A\beta$  peptides should be targeted to significantly reduce soluble  $A\beta$  load because of the relationship between these three. It has been hypothesized that by decreasing  $A\beta$  levels, soluble  $A\beta_O$  amounts are also reduced, in turn inducing the release of  $A\beta_O$  from plaques to restore the balance between  $A\beta_O$  in the plaques and the extracellular environment<sup>40</sup>.

The ability to identify and estimate the oligomerization effect through modelling suggested that these efforts to model the monomer pathway may also provide information on the higher ordered amyloid species. The ability to see this effect suggested that  $A\beta$  production inhibition by MBI-5 may also have the ability to draw down these forms as well as inhibit  $A\beta$  *de novo* production. In an APP transgenic mice study it has been demonstrated that BACE1 inhibition reduces amyloid plaque load (Kennedy and Hide, unpublished observations). This implies that if monomeric  $A\beta$  levels decrease as result of blocked  $A\beta$  production,  $A\beta_O$  dissociate to restore the equilibrium between monomeric  $A\beta$  and  $A\beta_O$ . To confirm this, incorporation of  $A\beta_O$  data into the model using rhesus data is ongoing.

A comprehensive model of the APP pathway describing the effects the BACEi MBI-5 has been established, taking into account the kinetics and interrelationships of sAPP $\alpha$ , sAPP $\beta$ , A $\beta$ 40 and A $\beta$ 42. The effect of BACE1 inhibition was incorporated in the model as inhibition of the formation rate of sAPP $\beta$ . As sAPP $\beta$  and C99 are both products of the same BACE1 cleavage step, the response of sAPP $\beta$  could be used as driver of  $A\beta$  response. However, sAPP $\beta$  and C99 could be subjected to different elimination processes as C99 remains membrane bound<sup>42</sup>. The fact that the Hill coefficient of the concentration response relationship slightly deviates from unity may be a reflection of this simplification of the underlying biological system. To adequately separate the sequential cleavage steps of BACE1 and  $\gamma$ -secretase from other processes involved, data from a  $\gamma$ -secretase inhibitor study in CMP rhesus<sup>18</sup> will be added to inform the model further (ongoing).

As BACE1 is the initiating enzyme in  $A\beta$  production, its inhibition has been proposed



to decrease the amount of cerebral  $A\beta$  and to subsequently prevent the development of  $A\beta$ -associated pathologies<sup>43</sup>. With the developed systems pharmacology model a deeper comprehension of the effects of BACEi on the APP processing pathway and the anticipated effect on  $A\beta_O$  was gained. Understanding these effects early in preclinical development could improve the anticipation of the magnitude of  $A\beta$  reducing effects in humans. The model forms the first step in developing a translational systems model to predict possible  $A\beta$  response of new drug candidates in human, based on their estimated potency in rhesus.

## References

1. Di Carlo, M., Giacomazza, D., & San Biagio, P.L. Alzheimer's disease: biological aspects, therapeutic perspectives and diagnostic tools. *J physics Condens matter an Inst Phys J*. 2012;24(24):244102.
2. Hardy, J. & Selkoe, D.J. The amyloid hypothesis of Alzheimer's disease: progress and problems on the road to therapeutics. *Science*. 2002;297(5580):353–6.
3. Benilova, I., Karran, E., & De Strooper, B. The toxic A $\beta$  oligomer and Alzheimer's disease: an emperor in need of clothes. *Nat Neurosci*. 2012;15(3):349–357.
4. Klein, W.L. Synaptotoxic amyloid- $\beta$  oligomers: a molecular basis for the cause, diagnosis, and treatment of Alzheimer's disease? *J Alzheimer's Dis*. 2013;33:S49–S65.
5. Savage, M.J., *et al*. A sensitive A $\beta$  oligomer assay discriminates Alzheimer's and aged control cerebrospinal fluid. *J Neurosci*. 2014;34(8):2884–97.
6. Esparza, T.J., *et al*. Amyloid-beta oligomerization in Alzheimer dementia vs. high pathology controls. *Ann Neurol*. 2013;73(1):104–119.
7. Mc Donald, J.M., *et al*. The presence of sodium dodecyl sulphate-stable A $\beta$  dimers is strongly associated with Alzheimer-type dementia. *Brain*. 2010;133:1328–41.
8. Yang, T., Hong, S., O'Malley, T., Sperling, R.A., Walsh, D.M., & Selkoe, D.J. New ELISAs with high specificity for soluble oligomers of amyloid  $\beta$ -protein detect natural A $\beta$  oligomers in human brain but not CSF. *Alzheimer's Dement*. 2013;9(2):99–112.
9. Esler, W.P. & Wolfe, M.S. A portrait of Alzheimer secretases - New features and familiar faces. *Science*. 2001;293(5534):1449–54.
10. Wiltfang, J., *et al*. Highly conserved and disease-specific patterns of carboxyterminally truncated A $\beta$  peptides 1-37/38/39 in addition to 1-40/42 in Alzheimer's disease and in patients with chronic neuroinflammation. *J Neurochem*. 2002;81(3):481–496.
11. Portelius, E., Mattsson, N., Andreasson, U., Blennow, K., & Zetterberg, H. Novel A Isoforms in Alzheimer's Disease - Their Role in Diagnosis and Treatment. *Curr Pharm Des*. 2011;17(25):2594–2602.
12. Husain, M.M., Kenneth, T., Siddique, H., & McClintock, S.M. Present and prospective clinical therapeutic regimens for Alzheimer's disease. *Neuropsychiatr Dis Treat*. 2008;4(4):765–777.
13. Yan, R. & Vassar, R. Targeting the  $\beta$  secretase BACE1 for Alzheimer's disease therapy. *Lancet Neurol*. 2014;13(3):319–329.
14. Lu, Y., *et al*. Cerebrospinal fluid amyloid- $\beta$  (A $\beta$ ) as an effect biomarker for brain A $\beta$  lowering verified by quantitative preclinical analyses. *J Pharmacol Exp Ther*. 2012;342(2):366–75.
15. Jack, C.R. & Holtzman, D.M. Biomarker modeling of Alzheimer's disease. *Neuron*. 2013;80(6):1347–1358.

16. Podlisny, M.B., Tolan, D.R., & Selkoe, D.J. Homology of the amyloid beta protein precursor in monkey and human supports a primate model for beta amyloidosis in Alzheimer's disease. *Am J Pathol.* 1991;138(6):1423–1435.
17. Gilberto, D.B., *et al.* An alternative method of chronic cerebrospinal fluid collection via the cisterna magna in conscious rhesus monkeys. *Contemp Top Lab Anim Sci.* 2003;42(4):53–59.
18. Cook, J.J., *et al.* Acute  $\gamma$ -secretase inhibition of nonhuman primate CNS shifts amyloid precursor protein (APP) metabolism from amyloid- $\beta$  production to alternative APP fragments without amyloid- $\beta$  rebound. *J Neurosci.* 2010;30(19):6743–50.
19. Lu, Y., *et al.* Cerebrospinal fluid  $\beta$ -amyloid turnover in the mouse, dog, monkey and human evaluated by systematic quantitative analyses. *Neurodegener Dis.* 2013;12(1):36–50.
20. Janson, J., *et al.* Population PKPD modeling of BACE1 inhibitor-induced reduction in  $A\beta$  levels in vivo and correlation to in vitro potency in primary cortical neurons from mouse and guinea pig. *Pharm Res.* 2014;31(3):670–83.
21. Parkinson, J., *et al.* Modeling of age-dependent amyloid accumulation and  $\gamma$ -secretase inhibition of soluble and insoluble  $A\beta$  in a transgenic mouse model of amyloid deposition. *Pharmacol Res Perspect.* 2013;1(2):e00012.
22. Liu, X., *et al.* Mechanistic pharmacokinetic-pharmacodynamic modeling of BACE1 inhibition in monkeys: development of a predictive model for amyloid precursor protein processing. *Drug Metab Dispos.* 2013;41(7):1319–28.
23. Potter, R., *et al.* Increased in vivo Amyloid- $\beta$ 42 production, exchange, and irreversible loss in Presenilin Mutations Carriers. *Sci Transl Med.* 2013;5(189):189ra77.
24. Danhof, M., Alvan, G., Dahl, S.G., Kuhlmann, J., & Paintaud, G. Mechanism-based pharmacokinetic-pharmacodynamic modeling - A new classification of biomarkers. *Pharm Res.* 2005;22(9):1432–7.
25. Danhof, M., De Jongh, J., De Lange, E.C., Della Pasqua, O., Ploeger, B.A., & Voskuyl, R.A. Mechanism-based pharmacokinetic-pharmacodynamic modeling: biophase distribution, receptor theory, and dynamical systems analysis. *Annu Rev Pharmacol Toxicol.* 2007;47:357–400.
26. Dobrowolska, J.A., *et al.* CNS amyloid- $\beta$ , soluble APP- $\alpha$  and - $\beta$  kinetics during BACE inhibition. *J Neurosci.* 2014;34(24):8336–8346.
27. Wu, G., Sankaranarayanan, S., Hsieh, S.H.K., Simon, A.J., & Savage, M.J. Decrease in brain soluble amyloid precursor protein  $\beta$  (sAPP $\beta$ ) in Alzheimer's disease cortex. *J Neurosci Res.* 2011;89(6):822–32.
28. Sankaranarayanan, S., *et al.* First demonstration of cerebrospinal fluid and plasma  $A\beta$  lowering with oral administration of a  $\beta$ -site amyloid precursor protein-cleaving enzyme 1 inhibitor in nonhuman primates. *J Pharmacol Exp Ther.* 2009;328(1):131–140.
29. Beal, S.L. NONMEM Users Guide: Introduction to Version VI. GloboMax

- ICON Development Solutions;Ellicott City, MD;2008.
30. Nelson, D.L. & Cox, M.M. *Lehninger Principles of Biochemistry* 3rd ed. Worth Publishers;New York;2000.
  31. Iwatsubo, T., Odaka, A., Suzuki, N., Mizusawa, H., Nukina, N., & Ihara, Y. Visualization of A $\beta$ 42(43) and A $\beta$ 40 in senile plaques with end-specific A $\beta$  monoclonals: evidence that an initially deposited species is A $\beta$ 42(43). *Neuron*. 1994;13(1):45–53.
  32. Cheng, X., Wu, J., Geng, M., & Xiong, J. The role of synaptic activity in the regulation of amyloid beta levels in Alzheimer's disease. *Neurobiol Aging*. 2014;35(6):1217–1232.
  33. Dobrowolska, J.A., *et al.* Diurnal patterns of soluble amyloid precursor protein metabolites in the human central nervous system. *PLoS One*. 2014;9(3):e89998.
  34. Murphy, M.P., Hickman, L.J., Eckman, C.B., Uljon, S.N., Wang, R., & Golde, E.T.  $\gamma$ -Secretase, evidence for multiple proteolytic activities and influence of membrane positioning of substrate on generation of amyloid  $\beta$  peptides of varying length. *J Biol Chem*. 1999;274(17):11914–11923.
  35. Dolev, I., *et al.* Spike bursts increase amyloid- $\beta$  40/42 ratio by inducing a presenilin-1 conformational change. *Nat Neurosci*. 2013;16(5):587–95.
  36. Jarrett, J.T., Berger, E.P., & Lansbury, P.T. The carboxy terminus of the  $\beta$  amyloid protein is critical for the seeding of amyloid formation: Implications for the pathogenesis of Alzheimer's disease. *Biochemistry*. 1993;32(18):4693–4697.
  37. Grüning, C.S.R., *et al.* The off-rate of monomers dissociating from amyloid- $\beta$  protofibrils. *J Biol Chem*. 2013;288(52):37104–11.
  38. Narayan, P., *et al.* The extracellular chaperone clusterin sequesters oligomeric forms of the amyloid- $\beta$ 1-40 peptide. *Nat Struct Mol Biol*. 2012;19(1):79–83.
  39. Sánchez, L., *et al.* A $\beta$ 40 and A $\beta$ 42 amyloid fibrils exhibit distinct molecular recycling properties. *J Am Chem Soc*. 2011;133(17):6505–6508.
  40. Rosenblum, W.I. Why Alzheimer trials fail: removing soluble oligomeric beta amyloid is essential, inconsistent, and difficult. *Neurobiol Aging*. 2014;35(5):969–974.
  41. Heuer, E., Rosen, R.F., Cintron, A., & Walker, L.C. Nonhuman primate models of Alzheimer-like cerebral proteopathy. *Curr Pharm Des*. 2012;18(8):1159–1169.
  42. Selkoe, D.J. Translating cell biology into therapeutic advances in Alzheimer's disease. *Nature*. 1999;399(6738 Suppl):A23–31.
  43. Cole, S.L. & Vassar, R. The basic biology of BACE1: A key therapeutic target for Alzheimer's disease. *Curr Genomics*. 2007;8(8):509–530.



---

# Chapter 3

## Supplemental Material

Adapted from supplement

Systems pharmacology analysis of the amyloid cascade following  $\beta$ -secretase inhibition enables the identification of an A $\beta$ 42 oligomer pool

**E.M.T. van Maanen, T.J. van Steeg, M.S. Michener, M.J. Savage, M.E. Kennedy, H.J. Kleijn, J.A. Stone, M. Danhof**

*The Journal of Pharmacology and Experimental Therapeutics*, 2016; 357(1): 205–16.





## Pharmacokinetic Data Analysis MBi-5

The exposure at the target site in the brain can rarely be quantified directly. In the cisterna magna ported (CMP) rhesus monkey model exposure can be measured in cerebrospinal fluid (CSF) in addition to plasma. The pharmacokinetics (PK) in plasma and CSF can be used to derive a measure of exposure at the target site. Therefore, a population PK model was developed that describes the PK of MBi-5 in plasma and CSF in CMP rhesus monkeys. The results of the PK analysis of MBi-5 were included in the subsequent PK-PD analysis.

The PK model was developed and fitted to the data by means of non-linear mixed effects modelling using the NONMEM software package version VI level 2 (see the Materials and Methods section in chapter 3).

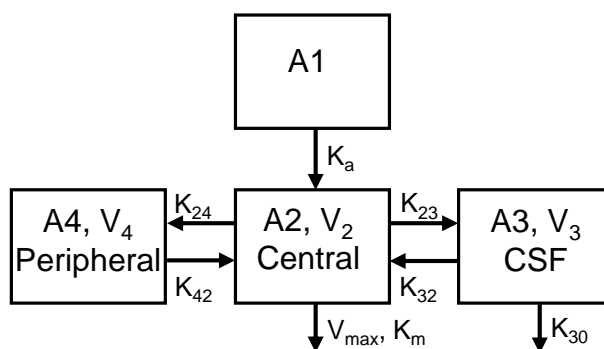


**Figure S3.1: Schematic of the population PK model for MBi-5, that comprised of a dose, central, peripheral and CSF compartment.**

Rate constants for the individual compartments are  $K_a$  (absorption),  $K_{24}$  (rate constant from central to peripheral),  $K_{42}$  (rate constant from peripheral to central),  $K_{23}$  (rate constant from central to CSF),  $K_{32}$  (rate constant from CSF to central).  $A1$ ,  $A2$ ,  $A3$ ,  $A4$ ,  $V_2$ ,  $V_3$  and  $V_4$  are amounts (A) and volume of distribution (V) of MBi-5 in dose, central, CSF and peripheral compartments, respectively.  $K_{30}$  is the elimination rate in CSF compartment.  $V_{max}$  is the maximum velocity;  $K_m$  is the Michaelis-Menten constant.

The compartmental PK model of MBi-5 was based on simultaneous analysis of plasma and CSF PK data. The PK profiles of MBi-5 in plasma and CSF were adequately described by a model containing three compartments: a central, peripheral and CSF compartment (Supplemental Figure S3.1). The CSF compartment is linked to the central compartment, with exchange determined by rate constants  $K_{32}$  and  $K_{23}$ . The model

considered elimination from the central and CSF compartment, where the elimination from the central compartment ( $K_{20}$ ) is described by the Michaelis-Menten equation (Equation S3.1).

$$K_{20} = \frac{V_{MAX}}{K_M + \frac{A_2}{V_2}} \quad (S3.1)$$

The rate of change in each compartment can be expressed as:

$$\frac{d}{dt}A_1 = -K_a \times A_1 \quad (S3.2)$$

$$\begin{aligned} \frac{d}{dt}A_2 = & K_a \times A_1 - K_{24} \times A_2 + K_{42} \times A_4 - K_{23} \times A_2 + K_{32} \times A_3 \\ & - \frac{V_{MAX} \times A_2}{K_M + \frac{A_2}{V_2}} \end{aligned} \quad (S3.3)$$

$$\frac{d}{dt}A_3 = K_{23} \times A_2 - K_{32} \times A_3 - K_{30} \times A_3 \quad (S3.4)$$

$$\frac{d}{dt}A_4 = K_{24} \times A_2 - K_{42} \times A_4 \quad (S3.5)$$

MBi-5 displayed nonlinear PK at different kinetic levels. The extent of the absorption decreased with an increase in dose ( $K_a$ , from 10.0 to 0.144 h<sup>-1</sup> for 10 and 125 mg/kg, respectively). The distribution to the CSF compartment appeared to be saturable, reflected in a decrease in the rate constant from the central to CSF compartment for the 125 mg/kg dose ( $K_{23}$ , from 0.000488 to 0.000116 h<sup>-1</sup>). Elimination was identified from the central and CSF compartment. As the elimination of MBI-5 from the central compartment followed Michaelis-Menten kinetics (Supplemental Equation S3.1) the clearance in the central compartment changed as function of time and concentration ( $CL_2 = K_{20}(t,C_p) \times V_2$ ). At the doses included in the current investigation, clearance in the CSF compartment ( $CL_3 = K_{30} \times V_3$ ) was approximately 10<sup>6</sup>-fold greater than clearance from the central

compartment, indicating that the CSF clearance route contributes remarkably.

Table S3.1 shows all PK parameter estimates. The volume of the CSF compartment could not be estimated and was fixed to a small value (0.0250 L). Interanimal variability was quantified for the volume of the central compartment ( $V_2$ ). Residual variability (proportional error) was higher for the CSF than for the plasma concentration (0.628 and 0.188 for CSF and plasma, respectively).

The developed PK model gives an adequate description of plasma and CSF concentration time profiles, as can be seen from plots of the simulated and observed concentrations *versus* time profiles with 90% confidence interval (Figure S3.2).

PK data from the CMP rhesus monkey show that there is substantial CSF exposure after oral dosing (10 fold lower than in plasma). The data suggest that MBi-5 concentrations in brain, expected to be in between plasma and CSF levels, are sufficient to adequately inhibit  $\beta$ -secretase activity in brain. The plasma and CSF concentrations *versus* time profiles predicted from the model had a good fit to the values observed in the rhesus monkeys. Thus, the model could serve as input for PD model analysis.

**Table S3.1: Population parameter estimates including coefficient of variation (CV%) for the PK model of MBi-5**

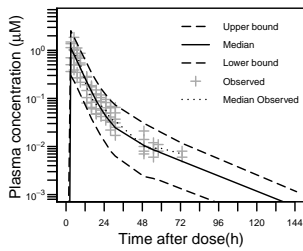
| PARAMETER                       | DESCRIPTION   | VALUE    | UNIT                 | CV%  |
|---------------------------------|---|----------|----------------------|------|
| <i>Structural parameters</i>    |   |          |                      |      |
| $V_2$                           | central volume                                      | 122      | L                    | 18.9 |
| $Q_4$                           | intercompartmental clearance                        | 2.01     | $L \cdot h^{-1}$     | 53.2 |
| $FV_4^a$                        | peripheral volume as fraction of central volume     | 0.488    |                      | 42.8 |
| $K_m$                           | Michaelis-Menten constant                           | 6.24     | $\mu M$              | 24.4 |
| $V_{max}$                       | maximum velocity                                    | 1.04     | $\mu M \cdot h^{-1}$ | 25.7 |
| $K_a$ dose10 <sup>b</sup>       | absorption rate dose10                              | 10.0     | $h^{-1}$             | -    |
| $K_a$ dose30                    | absorption rate dose30                              | 0.250    | $h^{-1}$             | 47.6 |
| $FK_a^c$                        | absorption rate dose125 as fraction of $K_a$ dose30 | 0.579    |                      | 37.0 |
| $K_{23}$                        | rate constant from central to CSF                   | 0.000488 | $h^{-1}$             | 37.7 |
| $FK_{23}$ dose 125 <sup>d</sup> | $K_{23}$ for dose125 as fraction                    | 0.239    |                      | 23.5 |
| $K_{30}$                        | elimination rate CSF compartment                    | 34.5     | $h^{-1}$             | 21.2 |
| $V_3^b$                         | volume CSF compartment                              | 0.0250   | L                    | -    |
| <i>Interanimal variability</i>  |   |          |                      |      |
| $\omega^2_{V_2}$                | Interanimal variability central volume              | 0.0612   |                      | 27.0 |
| <i>Residual error</i>           |   |          |                      |      |
| $\sigma^2_{plasma}$             | Residual variability plasma                         | 0.188    |                      | 10.5 |
| $\sigma^2_{CSF}$                | Residual variability CSF                            | 0.628    |                      | 26.4 |

<sup>a</sup>  $V_4 = V_2 \times FV_4$ .

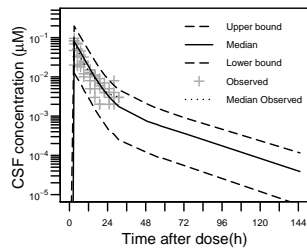
<sup>b</sup> Fixed.

<sup>c</sup>  $K_a$  dose125 =  $K_a$  dose30  $\times$   $FK_a$ .

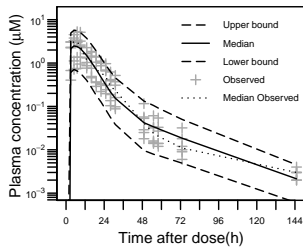
<sup>d</sup>  $K_{23}$  dose125 =  $K_{23}$   $\times$   $FK_{23}$ .



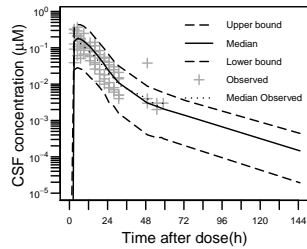
(A) 10 mg/kg MBI-5 plasma



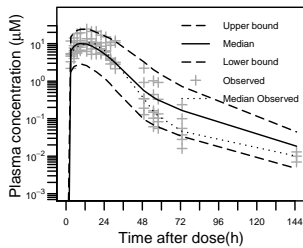
(B) 10 mg/kg MBI-5 CSF



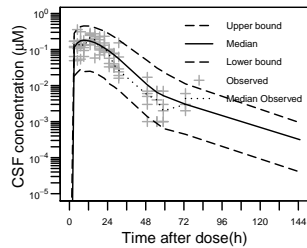
(C) 30 mg/kg MBI-5 plasma



(D) 30 mg/kg MBI-5 CSF



(E) 125 mg/kg MBI-5 plasma



(F) 125 mg/kg MBI-5 CSF

**Figure S3.2: Visual predictive check of plasma (left panels) and CSF (right panels) concentration time profile of MBI-5 in the rhesus with 90% confidence interval.**

The rhesus were administrated with 10 mg/kg (A) (B), 30 mg/kg (C) (D) and 125 mg/kg (E) (F) MBI-5. Observation sample size:  $n=102$  for plasma and CSF per dose from 6 monkeys collected over 7 days.

Plus-symbols represent observed measurements. Dotted line corresponds to the median observed profile. Solid lines show the median simulated profiles. The long-dashed lines correspond to the 90% prediction intervals obtained from 1000 individual simulated profiles.

